Inorg. Chem. **2009**, *48*, 2018−2027

Synthesis and Characterization of Ruthenium bis-Bipyridine Mono- and Disulfinato Complexes

Rowshan Ara Begum, Abdiaziz A. Farah, Howard N. Hunter, and A. B. P. Lever*

Department of Chemistry, York University, 4700 Keele Street, Toronto, Ontario M3J 1P3, Canada

Received October 5, 2008

Reaction of *cis*-$Ru(bpy)_2Cl_2$ with 1,2-benzenedithiol afforded a monosulfhydryl-monosulfinate complex, $[Ru(bpy)_2(S \cdot SO_2)]$ (**1**). Complex **1** readily undergoes oxidation when treated with 30% H_2O_2 and also upon exposure to atmospheric O_2 (rapidly in bright light) to afford the disulfinate complex, $[Ru(bpy)_2(SO_2.SO_2)]$ (**2**). Complexes **1** and **2** were studied using various analytical techniques including elemental analysis, UV−vis, mass spectroscopy, NMR, IR spectroscopy, cyclic voltammetry, X-ray crystallography (for **2**). Density functional theory computation was employed with extended charge decomposition and natural population analyses. The agreement between the observed electronic spectrum and that predicted by time dependent DFT, and between the observed infrared spectrum and that predicted by DFT, is truly exceptional. These molecules are relevant to the very unusual active site in the metalloenzyme *nitrile hydratase.*

Introduction

The extensive electronic coupling between the Ru(II) 4d electrons and π- and π^* orbitals in ruthenium(II) quinonoid complexes has been studied extensively both from an experimental and theoretical viewpoint. We have reported studies of a series of ruthenium complexes of the general formula $[Ru(bpy)_2(1,2(X \cdot Y)\text{-}C_6H_4]^{2+}$ and their oxidized and reduced derivatives, for X·Y = (O·O), (NH·NH), (NH·O), (NH·S).[1−14]

Our analyses of the electrochemistry, resonance Raman, and optical spectroscopic properties of these species, aided by density functional analysis, demonstrated considerable π-back-donation of the ruthenium dπ orbital to the lowest unoccupied molecular orbital (LUMO) which was mostly localized on the quinonoid ligand.

It would be interesting to study the corresponding $[Ru(bpy)_2(S \cdot S)]^{2+}$ species ((S·S) = 1,2-benzenedithiolate) but despite the extensive literature of dithiolene species[15−21] this particular ruthenium species is unknown. Tanaka has reported[22] the analogous $[Ru(CO)_2(tdt)(terpy)]$ where tdt is the 3,4-toluenedithiolate dianion and terpy is 2,2′:6′:2″-

* To whom correspondence should be addressed. E-mail: blever@yorku.ca.

(1) Haga, M.; Dodsworth, E. S.; Lever, A. B. P. *Inorg. Chem.* **1986**, *25*, 447–453.
(2) Stufkens, D. J.; Snoeck, T. L.; Lever, A. B. P. *Inorg. Chem.* **1988**, *27*, 953–956.
(3) Lever, A. B. P.; Auburn, P.; Dodsworth, E. S.; Haga, M.; Nevin, W. A. *J. Am. Chem. Soc.* **1988**, *110*, 8076–8084.
(4) Masui, H.; Lever, A. B. P.; Auburn, P. R. *Inorg. Chem.* **1991**, *30*, 2402–2410.
(5) Masui, H.; Lever, A. B. P.; Dodsworth, E. S. *Inorg. Chem.* **1993**, *32*, 258–267.
(6) Lever, A. B. P.; Masui, H.; Metcalfe, R. A.; Stufkens, D. J.; Dodsworth, E. S.; Auburn, P. R. *Coord. Chem. Rev.* **1993**, *125*, 317–331.
(7) Gorelsky, S. I.; Dodsworth, E. S.; Lever, A. B. P.; Vlcek, A. A. *Coord. Chem. Rev.* **1998**, *174*, 469–494.
(8) Lever, A. B. P.; Gorelsky, S. I. *Coord. Chem. Rev.* **2000**, *208*, 153–167.
(9) Gorelsky, S. I.; Lever, A. B. P. *J. Organomet. Chem.* **2001**, *635*, 187–196.
(10) Gorelsky, S. I.; Lever, A. B. P.; Ebadi, M. *Coord. Chem. Rev.* **2002**, *230*, 97–105.
(11) Gorelsky, S. I.; Lever, A. B. P. *Can. J. Anal. Sci. Spectrosc.* **2003**, *48*, 93–105.
(12) Lever, A. B. P.; Gorelsky, S. I. *Struct. Bonding (Berlin)* **2004**, *107*, 77–114.
(13) Rusanova, J.; Rusanov, E.; Gorelsky, S. I.; Christendat, D.; Popescu, R.; Farah, A. A.; Beaulac, R.; Reber, C.; Lever, A. B. P. *Inorg. Chem.* **2006**, *45*, 6246–6262.
(14) Kalinina, D.; Dares, C.; Kaluarachchi, H.; Potvin, P. G.; Lever, A. B. P. *Inorg. Chem.* **2008**, *47*, 10100–10126.
(15) Burns, R. P.; McAuliffe, C. A. *Adv. Inorg. Chem. Radiochem.* **1979**, *22*, 303–48.
(16) Mahadevan, C. *J. Crystallogr. Spectrosc. Res.* **1986**, *16*, 347–416.
(17) Clemenson, P. I. *Coord. Chem. Rev.* **1990**, *106*, 171–203.
(18) Rauchfuss, T. B. *Prog. Inorg. Chem.* **2003**, *52*, 1–54.
(19) Beswick, C. L.; Schulman, J. M.; Stiefel, E. I. *Prog. Inorg. Chem.* **2003**, *52*, 55–110.
(20) Kirk, M. L.; McNaughton, R. L.; Helton, M. E. *Prog. Inorg. Chem.* **2003**, *52*, 111–212.
(21) Zanello, P.; Grigiotti, E. In *New Trends in Molecular Electrochemistry*; Fontismedia: New York, 2004; pp 3−70.
(22) Sugimoto, H.; Wada, H.; Wakatsuki, Y.; Wada, T.; Tanaka, K. *Chem. Lett.* **2002**, 634–635.

10.1021/ic801898t CCC: $40.75
Published on Web 01/27/2009

Scheme 1. Synthetic Scheme for the Preparation of **1** and **2**[a]

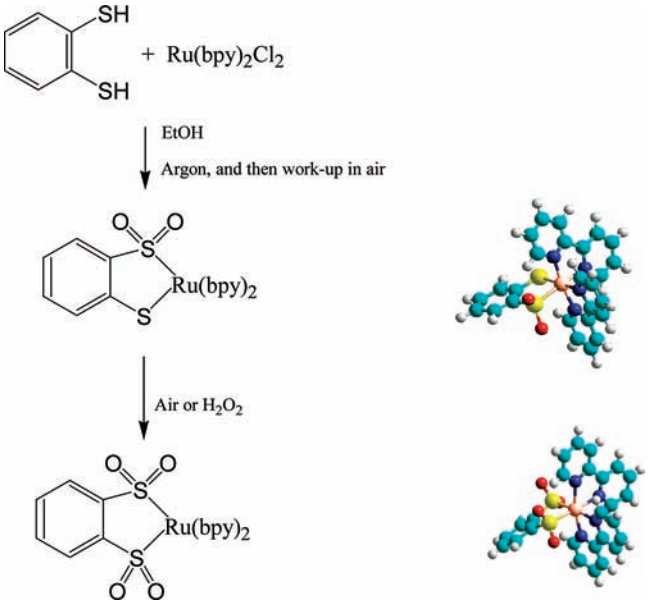

[a] Structures show DFT optimized geometries for **1**, and X-ray data for **2**, for illustration purposes.

terpyridine. He also reported[23] the analogous two electron oxidized species $[Ru(H_2O)(tdtQ)(terpy)]^{2+}$. In attempting to prepare benzenedithiolate species we have isolated and characterized $[Ru(bpy)_2(S\cdot SO_2)]$ (**1**) and its oxidized product $[Ru(bpy)_2(SO_2\cdot SO_2)]$ (**2**) (Scheme 1) where $(S\cdot SO_2)$ is the dianion of *o*-benzene monosulfhydryl monosulfinic acid and $(SO_2\cdot SO_2)$ is the dianion of *o*-benzenedisulfinic acid (Scheme 1). Of these free acids, only the latter is known.[24−27] Oxidation of *o*-dithiolates (S·S) bound to metal ions such iron(II), nickel(II), palladium(II), platinum(II), and ruthenium(II) is known to lead to metal−sulfur bound sulfhydryl monosulfinates $(S\cdot SO_2)$ and disulfinates $(SO_2\cdot SO_2)$[22,28−39] but rarely to mono- $(S\cdot SO)$ or disulfenates $(SO\cdot SO)$.[35,40−42] However these molecules are relevant to the very unusual active site in the metalloenzyme *nitrile hydratase* which contains an iron atom bound simultaneously[30,36,43] to −S, −SO and $-SO_2$, and indeed −NO.

Experimental Section

Synthetic Procedures. Methods and Materials. All reagents were obtained from Aldrich Chemicals Canada, Fluka Inc., Alfa Aesar, or the Johnson Matthey Company. Reagent grade solvents were obtained from Caledon and BDH Inc. All chemicals and solvents were purified where necessary according to conventional laboratory techniques. Infrared spectra were recorded as KBr pellets with a Mattson 3000 Fourier Transform Infrared Spectrophotometer. ^1H and ^{13}C NMR were acquired on a Bruker DRX 600 NMR spectrometer using either a TXI-Z or broadband-observe 5 mm probes. Two dimensional experiments were used directly from the standard pulse program library without modification. The NMR solvent DMSO-d_6 was manufactured by Cambridge Isotope Laboratories. Signals are described as singlets (s), doublets (d), doublets of doublets (dd), triplets (t), quartets (q), broad (br), or multiplets (m).

Calculations. Density functional theory (DFT) calculations utilized the Gaussian 03 (Revision C.02) and Gaussian 03W (Revision v.6) programs.[44] Optimized geometries were calculated using the popular B3LYP functional[45] with the TZVP (triple-ζ valence polarization) basis set[46,47] for all elements except Ruthenium where the double-ζ DGDZVP basis set[48,49] was used. Initial calculations using the LANL2DZ basis set[50−53] were less successful. Tight SCF convergence criteria (10^{-8} a.u.) were used for all calculations. Vibrational frequency calculations were performed to ensure that the stationary points were minima. Under the computational conditions, the wave functions were stable.

Molecular orbital (MO) compositions and the overlap populations between molecular fragments were calculated using the AOMix program[9,54] using the Mulliken scheme.[55−58] Atomic charges were calculated using the Mulliken and natural population analysis methods (MPA and NPA, respectively) as implemented in Gaussian 03. The

(23) Diógenes, I. C. N.; de Sousa, J. R.; de Carvalho, I. M. M.; Temperini, M. L. A.; Tanaka, A. A.; de Sousa Moreira, I. *J. Chem. Soc., Dalton Trans.* **2003**, 2231–2236.
(24) Hansen, H. C.; Kice, J. L. *J. Org. Chem.* **1983**, *48*, 2943–2948.
(25) Kice, J. L.; Liao, S. *J. Org. Chem.* **1981**, *46*, 2691–2694.
(26) Hendrickson, J. B.; Okano, S.; Bloom, R. K. *J. Org. Chem.* **1969**, *34*, 3434–3438.
(27) Hurtley, Wm. R. H.; Smiles, S. *J. Chem. Soc.* **1926**, 1821–1828.
(28) Makedonas, C.; Mitsopoulou, C. A. *Spectrochim. Acta, Part A* **2006**, *64*, 918–30.
(29) Lee, C.-M.; Hsieh, C.-H.; Dutta, A.; Lee, G.-H.; Liaw, W.-F. *J. Am. Chem. Soc.* **2003**, *125*, 11492–11493.
(30) Nagashima, S.; Nakasako, M.; Dohmae, N.; Tsujimura, M.; Takio, K.; Odaka, M.; Yohda, M.; Kamiya, N.; Endo, I. *Nat. Struct. Biol.* **1998**, *5*, 347–351.
(31) Xi, R.; Abe, M.; Suzuki, T.; Nishioka, T.; Isobe, K. *J. Organomet. Chem.* **1997**, *549*, 117–125.
(32) Connick, W. B.; Gray, H. B. *J. Am. Chem. Soc.* **1997**, *119*, 11620–11627.
(33) Grapperhaus, C. A.; Darensbourg, M. Y. *Acc. Chem. Res.* **1998**, *31*, 451–459.
(34) Grapperhaus, C. A.; Poturovic, S.; Mashuta, M. S. *Inorg. Chem.* **2005**, *44*, 8185–8187.
(35) Cornman, C. R.; Stauffer, T. C.; Boyle, P. D. *J. Am. Chem. Soc.* **1997**, *119*, 5986–5987.
(36) Bourles, E.; de Sousa, R. A.; Galardon, E.; Giorgi, M.; Artaud, I. *Angew. Chem.* **2005**, *117*, 6318–6321.
(37) Von Poelhsitz, G.; Rodrigues, B. L.; Batista, A. A. *Acta Crystallogr., Sect. C: Cryst. Struct. Commun.* **2006**, *C62*, m424−m427.
(38) Dilworth, J. R.; Zheng, Y.; Lu, S.; Wu, Q. *Transition Met. Chem.* **1992**, *17*, 364–368.
(39) Grapperhaus, C. A.; Darensbourg, M. Y.; Sumner, L. W.; Russell, D. H. *J. Am. Chem. Soc.* **1996**, *118*, 1791–1792.
(40) Buonomo, R. M.; Font, I.; Maguire, M. J.; Reibenspies, J. H.; Tuntulani, T.; Darensbourg, M. Y. *J. Am. Chem. Soc.* **1995**, *117*, 963–73.
(41) Schrauzer, G. N.; Zhang, C.; Chadha, R. *Inorg. Chem.* **1990**, *29*, 4104–4107.
(42) Tuntulani, T.; Musie, M.; Reibenspies, J. H.; Darensbourg, M. Y. *Inorg. Chem.* **1995**, *34*, 6279–6286.
(43) Kung, I.; Schweitzer, D.; Shearer, J.; Taylor, W. D.; Jackson, H. L.; Kovacs, J. A. *J. Am. Chem. Soc.* **2000**, *122*, 8299–8300.
(44) Frisch, M. J.; Trucks, G. W.; Schlegel, H. B. et al. *Gaussian 03, Revision C*; Gaussian, Inc.: Wallingford, CT, 2004.
(45) Lee, C.; Yang, W.; Parr, R. G. *Phys. Rev. B* **1988**, *37*, 785–789.
(46) Schaefer, A.; Horn, H.; Ahlrichs, R. *J. Chem. Phys.* **1992**, *97*, 2571.
(47) Schafer, A.; Huber, C.; Ahlrichs, R. *J. Chem. Phys.* **1994**, *100*, 5829.
(48) Godbout, N.; Salahub, D. R.; Andzelm, J.; Wimmer, E. *Can. J. Chem.* **1992**, *70*, 560.
(49) Sosa, C.; Andzelm, J.; Elkin, B. C.; Wimmer, E.; Dobbs, K. D.; Dixon, D. A. *J. Phys. Chem.* **1992**, *96*, 6630.
(50) Dunning, T. H., Jr.; Hay, P. J. *Modern Theoretical Chemistry*; Schaefer, H.F., Ed.; Plenum: New York, 1976; Vol. *3*, p 1.
(51) Hay, P. J.; Wadt, W. R. *J. Chem. Phys.* **1985**, *82*, 270–283.
(52) Hay, P. J.; Wadt, W. R. *J. Chem. Phys.* **1985**, *82*, 284–298.
(53) Hay, P. J.; Wadt, W. R. *J. Chem. Phys.* **1985**, *82*, 299–310.
(54) Gorelsky, S. I. *AOMix-CDA Program for Molecular Orbital Analysis*; University of Ottawa: Ottawa, Canada, 2008; http://www.sg-chem.net/.
(55) Mulliken, R. S. *J. Chem. Phys.* **1955**, *23*, 2338–2342.
(56) Mulliken, R. S. *J. Chem. Phys.* **1955**, *23*, 1833–1840.
(57) Mulliken, R. S. *J. Chem. Phys.* **1955**, *23*, 2343–2346.
(58) Mulliken, R. S. *J. Chem. Phys.* **1955**, *23*, 1841–1846.

analysis of the MO compositions and the charge decomposition analysis were performed using AOMix-CDA.[59] The PCM model[60−62] was used to model solvation assuming acetonitrile as solvent.

Time-dependent DFT (TD-DFT)[63−66] was used to calculate the energies and intensities of the 100 lowest-energy electronic transitions of both complexes. These were converted with the SWizard program[67] into simulated spectra as described before,[68] using Gaussian functions with half-widths as noted in the figure legends.

X-ray Data for Species 2. A single yellow needle crystal of dimensions 0.22 × 0.08 × 0.08 mm was used for X-ray diffraction studies. X-ray diffraction data were collected at 150(1) K on a Nonius Kappa CCD diffractometer, using graphite monochromated Mo Kα radiation ($\lambda = 0.71073$ Å) with a ω scan mode. A total of 11136 reflections collected in the $2.5° < \theta < 29.4°$ range, of which 6100 were independent, and 4058 with $I > 2\sigma(I)$ were used for subsequent structure refinement. The structure was solved and refined using the SHELXTL\PC V6.1 package.[69] Full-matrix least-squares refinement of the initial structure solution obtained by direct methods was performed on F^2. All non-hydrogen atoms were refined anisotropically. Hydrogen atoms were added in calculated positions using the riding model approximation with $U_{iso}(H) = 1.2U_{eq}(C)$ for parent aromatic carbon atoms and $1.5U_{eq}(C)$ for parent methyl carbon atoms. The final structure refinement converged to $R = 0.0569$ and $wR = 0.1311$, $w = 1/[\sigma^2(F_o^2) + (0.0811P)^2]$, where $P = (F_o^2 + 2F_c^2)/3$. The largest residual differential peak was 1.440 e·Å^{-3}, the largest hole −1.966 e·Å^{-3}, $(\Delta/\sigma) = 0.000$. The goodness-of-fit on $F^2 = 1.050$.

***cis*-Ru(bpy)$_2$Cl$_2$** was prepared according to the literature[70] by Sullivan et al.

[Ru(bpy)$_2$(S·SO$_2$)] (**1**): 1,2-benzenedithiol (227.0 mg (1.43 mmol) was dissolved in anhydrous ethanol (20 mL) under an inert atmosphere. *cis*-Ru(bpy)$_2$Cl$_2$ (357.0 mg (0.70 mmol)) was gradually added to the ethanol solution which was then refluxed overnight. Further processing was carried out in air. The color of the reaction mixture turned deep green. After cooling to room temperature, dichloromethane (30 mL) was added to the reaction mixture. This solution was then washed with 2% $NaHCO_3$ solution (2 × 30 mL) followed by subsequent extraction with additional CH_2Cl_2. The solution was dried over $MgSO_4$ and, following removal of the solid $MgSO_4$, the solution was evaporated to dryness. The crude product was chromatographed on a silica gel column using a CH_2Cl_2:MeOH (1:1) mixture. Compound **1** was isolated as a deep green band (this was the second green band). Yield: 60 mg (14.3%).

^{1}H NMR (600 MHz, DMSO-d$_6$, RT, δ/ppm): δ 10.38 (d, J = 4.9 Hz, 1H, H^3 or H$^{3'}$), 9.53 (d, J = 4.9 Hz, 1H, H^3 or H$^{3'}$), 8.56 (d, 1H, H^{12} or H$^{12'}$), 8.53 (d, 1H, H^6 or H$^{6'}$), 8.52 (d, 2H, (H^6 or H$^{6'}$) and (H^{12} or H$^{12'}$)), 7.98 (dd, 1H, H^5 or H$^{5'}$), 7.94 (dd, 1H, H^5 or H$^{5'}$), 7.93 (dd, 1H, H^{10} or H$^{10'}$), 7.92 (dd, 1H, H^{10} or $^{10'}$), 7.73 (d, J = 4.9 Hz, 1H, H^9 or H$^{9'}$), 7.52 (dd, 1H, H^4 or H$^{4'}$), 7.50 (d, 1H, H^9 or H$^{9'}$), 7.50 (dd, 1H, H^4 or H$^{4'}$), 7.34 (dd, 1H, H^{10} or H$^{10'}$), 7.33 (dd, 1H, H^{10} or H$^{10'}$), 7.15 (d, J = 7.6 Hz, 1H, H^{15} or H^{18}), 7.12 (d, J = 7.6 Hz, 1H, H^{15} or H^{18}), 6.81 (dd, J = 7.0 and 7.6 Hz, 1H, H^{16} or H^{17}), 6.72 (dd, J = 7.0 and 7.6 Hz, 1H, H^{16} or H^{17}). ^{13}C NMR (125 MHz, DMSO-d$_6$, RT, δ/ppm): δ 158.1 (s, C^{1}or C$^{1'}$ or C^7 or C$^{7'}$), 157.7 (s, C^7 or C$^{7'}$), 156.7 (s, C^{1}or C$^{1'}$), 156.5 (s, C^{13}or C^{14}), 155.7 (s, C^7 or C$^{7'}$), 154.6 (s, C^3 or C$^{3'}$), 153.2 (s, C^3 or C$^{3'}$), 150.2 (s, C^9 or C$^{9'}$), 149.6 (s, C^9 or C$^{9'}$), 146.0 (s, C^{13}or C^{14}), 136.8 (s, C^{12} or C$^{12'}$), 135.9 (s, C^{12} or C$^{12'}$), 135.4 (s, C^6 or C$^{6'}$), 134.9 (s, C^6 or C$^{6'}$), 128.2 (s, C^{15} or C^{18}), 127.6 (s, C^{16} or C^{17}), 126.1 (s, C^{10} or C$^{10'}$), 125.9 (s, C^{10} or C$^{10'}$), 125.6 (s, C^{4}or C$^{4'}$), 125.3 (s, C^{4}or C$^{4'}$), 122.8 (s, (C^{5}or C$^{5'}$) and C^{11}or C$^{11'}$), 123.0 (s, C^{5}or C$^{5'}$), 122.6 (s, C^{11}or C$^{11'}$), 121.0 (s, C^{15} or C^{18}), 120.0 (s, C^{16} or C^{17}).

Mass spectra: matrix-assisted laser desorption ionization (MALDI): 585.8 (calcd. 586). Electrospray ionization-mass spectroscopy (ESI-MS) (high resolution): m/z = 587 (M+H)$^+$ UV−vis. in DMF: wavelength (ε, L mol^{-1} cm^{-1}): λ (nm): 636 (1730), 464 (7120). Anal. Calcd. For $C_{26}H_{20}N_4S_2O_2Ru$: C, 53.32, H, 3.44, N 9.57. Found: C, 52.88, H, 3.42 N, 9.31%.

Ru(bpy)$_2$(SO$_2$·SO$_2$) (**2**): Hydrogen peroxide (30% H_2O solution) was added slowly to a green suspension of **1** (50 mg, 0.08 mmol) in *N*,*N*′-dimethylformamide (∼5 mL) (partially soluble). The color started to turn yellowish and finally gave a bright yellow clear solution upon addition of a slight excess of H_2O_2. The solution was kept several days at room temperature to afford bright yellow colored crystals. The addition of a large excess of H_2O_2 produces a yellow powder instantly. The excess solution was decanted from the top, and the product washed carefully with water and dried under vacuo. Yield: 20 mg (37.5%).

^{1}H NMR (600 MHz, DMSO-d$_6$, RT, δ/ppm): δ 9.86 (d, J = 6.0 Hz, 2H, H^3 and H$^{3'}$), 8.65 (d, J = 7.6 Hz, 2H, H^{12} and H$^{12'}$), 8.62 (d, J = 7.6 Hz 2H, H^6 and H$^{6'}$), 8.09 (dd, 2H, H^5 and H$^{5'}$), 8.07 (dd, 2H, (H^{11} and H$^{11'}$), 7.57 (d, 2H, H^9 or H$^{9'}$), 7.56 (dd, 2H, H^{10} and H$^{10'}$), 7.52 (d, 2H, H^{15} and H^{18}), 7.44 (dd, 2H, H^4 and $^{4'}$), 7.39 (dd, 2H, H^{16} or H^{17}). ^{13}C NMR (125 MHz, DMSO-d$_6$, RT, δ/ppm): δ 157.0 (s, C^1 and C$^{1'}$), 156.0 (s, C^7 and C$^{7'}$), 153.8 (s, C^3 and C$^{3'}$), 152.0 (s, C^{13} and C^{14}), 150.0 (s, C^9 and C$^{9'}$), 138.1 (s, C^{11} and C$^{11'}$), 137.2 (s, C^5 and C$^{5'}$), 129.7 (s, C^{16} and C^{17}), 126.4 (s, C^{10} and C^{10}), 126.0 (s, C^4 and C$^{4'}$), 123.1 (s, C^6 and C$^{6'}$), 122.9 (s, C^{12} and C$^{12'}$), 119.5 (s, C^{15} and C^{18}).

ESI-MS parent ion 640 m/z (M + Na)$^+$; calcd. 640). UV−vis in DMF: wavelength (ε, L mol^{-1} cm^{-1}): λ (nm) 410 (5840). Anal. Calcd. For $C_{26}H_{20}N_4S_2O_4Ru·4H_2O$: C, 45.28, H, 4.09, N 8.12, Found C, 44.50, H, 4.01 N, 7.94%.

Results and Discussion

Reaction of *cis*-Ru(bpy)$_2$Cl$_2$ with 1,2-benzenedithiol afforded a deep green mixture under argon. Two green bands were observed during chromatography in the presence of air. Considerable effort was expended to purify both products. The first green band gave complex NMR spectra and was likely the desired dithiolate, but we were unsuccessful in purifying it even when such attempts were carried out under anaerobic conditions. Purification of the second band off the column led to the green complex, [Ru(bpy)$_2$(S·SO$_2$)] (**1**). In the high resolution mass spectrum of **1**, the parent ion

(59) Gorelsky, S. I.; Ghosh, S.; Solomon, E. I. *J. Am. Chem. Soc.* **2006**, *128*, 278.
(60) Neese, F. *Coord. Chem. Rev.* **2009**, in press (doi: 10.1016/j.ccr.2008.05.014).
(61) Noodleman, L.; Lovell, T.; Han, W. G.; Liu, T.; Torres, R. A. In *Comprehensive Coordination Chemistry II*; Elsevier: Oxford, 2003; pp 491−510.
(62) Bickelhaupt, F. M.; Baerends, E. J. *Reviews in Computational Chemistry*; Lipkowitz, K. B.; Boyd, D. R. E., Eds.; Wiley: New York, 2000; Vol. *15*, pp 1−86.
(63) Stratmann, R. E.; Scuseria, G. E.; Frisch, M. J. *J. Chem. Phys.* **1998**, *109*, 8218.
(64) Bauernschmitt, R.; Ahlrichs, R. *Chem. Phys. Lett.* **1996**, *256*, 454.
(65) Casida, M. E.; Jamorski, C.; Casida, K. C.; Salahub, D. R. *J. Chem. Phys.* **1998**, *108*, 4439.
(66) Zhou, X.; Pan, Q.-J.; Li, M.-X.; Xia, B.-H.; Zhang, H.-X. *J. Mol. Struct. THEOCHEM* **2007**, *822*, 65–73.
(67) Gorelsky, S. I. *SWizard program, CCRI*; University of Ottawa: Ottawa, Canada, 2008; http://www.sg-chem.net/.
(68) Gorelsky, S. I. *Comprehensive Coordination Chemistry-II*; Elsevier Science Publishers: 2004; Chapter *2.51*, pp 651−660.
(69) Sheldrick, G. M. *SHELXTL\PC*, V6.1; Bruker Analytical X-ray Systems: Madison, WI, 2001.
(70) Johnson, E. S.; Sullivan, B. P.; Salmon, D. J.; Adeyemi, A.; Meyer, T. J. *Inorg. Chem.* **1978**, *17*, 2211.

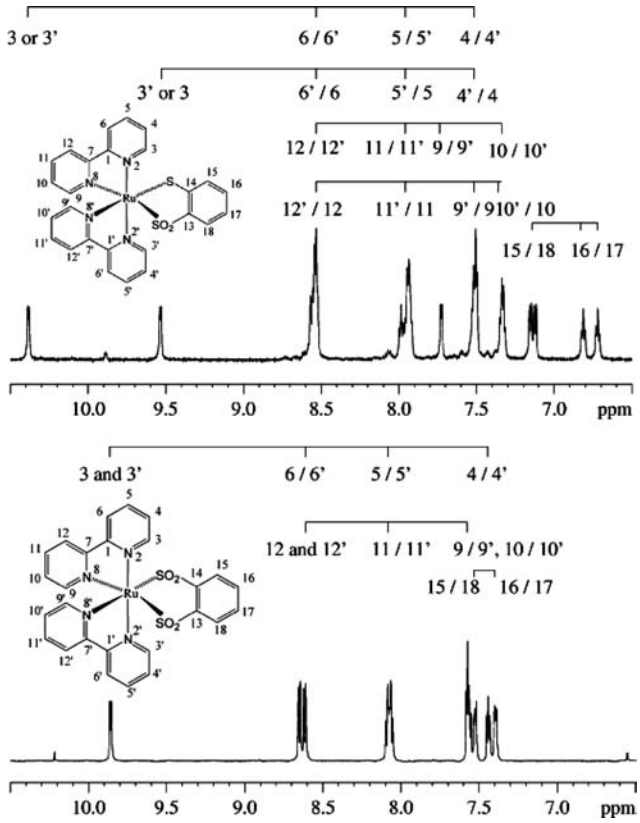

Figure 1. 600 MHz NMR spectra of complex 1 (top) and complex 2 (bottom). The groupings for the aromatic spin systems are indicated above each spectrum.

peak at $m/z = 587$ (and microanalytical data) was consistent with the presence of $[Ru(bpy)_2(S\cdot SO_2)]$ (**1**) not the initially desired dithiolate $[Ru(bpy)_2(S\cdot S)]$. It is probable that atmospheric oxygen oxidized the initial dithiolate.[32,42]

The mass spectroscopic and analytical evidence does not clarify whether the structure **1** is $[Ru(bpy)_2(S\cdot SO_2)]$ or $[Ru(bpy)_2(SO\cdot SO)]$, though the latter is unlikely on the basis of the previous literature. To confirm the structure of **1**, several 2D NMR experiments were performed to assist in the identification of the bipyridine rings and the S and SO_2 substituted aromatic ring. These assignments were based upon analysis of the ^1H NMR spectrum (Figure 1) in comparison with the homonuclear 2D $^1H-^1H$ COSY and TOCSY and heteronuclear 2D $^1H-^{13}C$ HSQC, HSQC-TOCSY, and HMBC spectra. Overall, the ^1H NMR spectrum of **1** reflects 10 unique proton resonances, indicative of an asymmetric complex.

The aromatic proton resonances for the disubstituted aromatic ring could readily be recognized from the 2D TOCSY spectrum in conjunction with peak integration and J-coupling analysis. The appearance of four separate resonances for the aromatic protons is suggestive of a lack of symmetry caused by two different substituents (S and SO_2) on the aromatic phenyl ring. The identification of the ^{13}C chemical shifts of the methine and quaternary phenyl resonances from the 2D HSQC and HMBC experiments shows a difference of 10.5 ppm for the two quaternary ^{13}C resonances (146.0 and 156.5 ppm) and 4 different shift values for the methine protons. Since the shielding of the ^{13}C nuclei

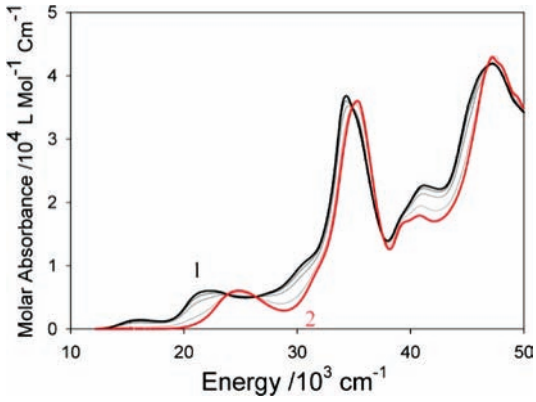

Figure 2. Electronic spectroscopic changes, with time, of $[Ru(bpy)_2(S\cdot SO_2)]$ (**1**, black) to $[Ru(bpy)_2(SO_2SO_2)]$ (**2**, red) in CH_3CN, in air, with irradiation of light. The reaction was completed within ~20 min.

by the valence electrons tends to reduce the importance of contributions from diamagnetic anisotropy to the ^{13}C shift, the difference in quaternary ^{13}C shifts may be attributed to inductive effects from both S-substituents in differing oxidation states. The lack of symmetry observed in the proton spectrum of the bipyridine rings also supports the lack of symmetry in the molecule as expected[71] for **1.**

Complex **1** is fairly stable in air in the solid state at room temperature, but a green colored solution of this complex undergoes oxidation slowly in air (more rapidly upon irradiation with white light[32,42]), and rapidly with addition of hydrogen peroxide, to afford the yellow colored complex, **2** (Figure 2, Scheme 1).

The electronic spectrum of **1** displays two weak absorption bands in the range 10−25,000 cm^{-1} which are replaced, upon oxidation, by a single band at about 24,000 cm^{-1}, in the spectrum of species **2**. The presence of at least two isosbestic points, during this oxidation process, eliminates the probability of existence of any intermediate Ru(III) species in the conversion process unless the rate of reaction of the Ru(III) intermediate is so fast that it never accumulates. This differs from a previous study of a related compound[34] where a Ru(III) intermediate was clearly observed. The ^1H and ^{13}C chemical shifts for the di-(SO_2)-substituted aromatic ring of **2** were studied for comparison with compound **1**. Only two different ^1H and three different ^{13}C resonances were observed with the two quaternary ^{13}C nuclei assigned to 151.95 ppm. The ^1H and ^{13}C shifts and the proton resonances assigned to the bipyridine rings in compound **2** are consistent with a symmetrical 1,2-disubstituted ring with identical substituents and C_2 symmetry for the complex overall in solution; packing forces in the solid appear to prevent C_2 symmetry.

The crystal structure of species **2** was obtained confirming the disulfinate structure ($SO_2\cdot SO_2$). Note that the benzene ring of the ($SO_2\cdot SO_2$) ligand is canted out of the S−Ru−S plane. Crystallographic information is shown in Table 1, selected bond lengths and angles in Table 2, and the Oak Ridge Thermal Ellipsoid Plot (ORTEP) diagram in Figure 3. Note that hydrogen peroxide oxidation of **1** does not lead

(71) Birchall, J. D.; O'Donoghue, T. D.; Wood, J. R. *Inorg. Chim. Acta* **1979**, *37*, L461-3.

Table 1. Summary of Crystallographic Data and Refinement Results for $[Ru(bpy)_2(SO_2 \cdot SO_2)] \cdot DMF$ (**2**)

empirical formula	$C_{29}H_{27}N_5O_5RuS_2$
Fw	690.75
crystal system	triclinic
space group	$P\bar{1}$
temp, K	150(1)
wavelength (Å)	0.71073
crystal size (mm^3)	0.22 × 0.08 × 0.08
unit cell dimensions	
a, Å	9.3320(4)
b, Å	11.9851(5)
c, Å	12.7966(4)
α, deg	99.3380(19)
β, deg	93.988(2)
γ, deg	100.8960(19)
volume, $Å^3$	1379.37(9)
density (calcd)	1.663 Mg/m^3
Z	2
abs coeff, mm^{-1}	0.771
F(000)	704
θ range, deg	2.55−27.49
max. and min. transmission	0.945 and 0.694
absorption correction	semiempirical from equivalents
refinement method	full-matrix least-squares on F^2
data/ restrains /parameters	6100/ 0/ 379
index ranges	
	$-12 \le h \le 12$
	$-15 \le k \le 15$
	$-16 \le l \le 16$
completeness to *θ* (%)	98.7
reflns collected	11136
independent reflns	6100 [*R*(int) = 0.0669]
final *R* indices ($I > 2\sigma(I)$)	R1 = 0.0552, wR2 = 0.1264
R indices (all data)	R1 = 0.1048, wR2 = 0.1567
GOF on F^2	1.049
largest diff. peak and hole (e $Å^{-3}$)	1.443 and −1.700

Table 2. Selected Bond Distances (Å) for $[Ru(bpy)_2(SO_2.SO_2)] \cdot DMF$ (**2**)

bond	distance (Å)
Ru(1)−N(3)	2.086(4)
Ru(1)−N(1)	2.094(4),
Ru(1)−N(4)	2.126(4),
Ru(1)−N(2)	2.129(3)
Ru(1)−S(1)	2.2536(13)
Ru(1)−S(2)	2.2680(12)
S(1)−O(1)	1.476(3)
S(1)−O(2)	1.476(4)
S(2)−O(3)	1.478(3)
S(2)−O(4)	1.483(4)
S(2)−C(21)	1.807
S(1)−C(22)	1.817

to a disulfonato derivative ($SO_3 \cdot SO_3$) as is the case with an analogous nickel(II) complex.[72] Such a species would necessitate a Ru−O bond which is less favorable, for ruthenium, than the Ru−S bond in **2**.

The ESI-MS analysis of compound **2** displays a parent ion peak at $m/z = 641$, which is assigned to the anticipated disulfinate complex associated with sodium ion (from the matrix used). Thus the NMR, mass spectra, X-ray (**2**), and analytical data support the formulations of these species as **1** $[Ru(bpy)_2(S \cdot SO_2)]$ and **2** $[Ru(bpy)_2(SO_2.SO_2)]$; these neutral species formally contain Ru(II) and the dianionic ligands. The oxidation of sulfides to sulfoxides and sulfones by hydrogen peroxide is well-known but usually requires a

(72) Cocker, M. T.; Bachman, R. E. *Chem. Commun. (Cambridge)* **1999**, 875–876.

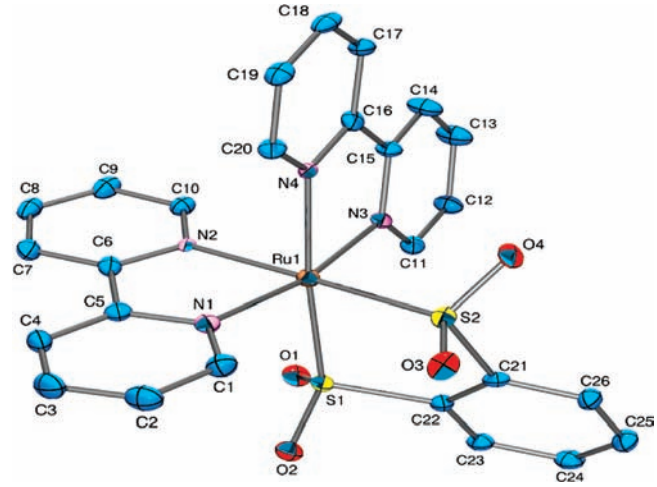

Figure 3. ORTEP diagram of species **2**. Hydrogen atoms are not shown.

Table 3. Selected Bond Distances in DFT Geometry Optimized Structures (Å) B3LYP/TZVP and B3LYP/DGDZVP, PCM CH_3CN)

	Ru−N	Ru−S	Ru−SO2	S−O	C−S	C−SO2
1 $(S \cdot SO_2)$	2.12−2.15	2.45	2.36	1.53	1.78	1.84
2 $(SO_2 \cdot SO_2)$	2.14,2.15		2.36	1.52,1.53		1.85

catalyst.[73−77] Likely, in this case, the ruthenium center provides an autocatalytic process.

Theoretical Aspects: Density Functional Theory Calculations, Molecular Orbitals, Electrochemistry and Vibrational and Electronic Spectroscopic Assignments. These very electron rich sulfur ligands have rarely been studied, especially the $S \cdot SO_2$ ligand, and therefore we provide a fairly in-depth analysis of their properties. Both ligands (referred to henceforth generally as S-ligands) carry two net negative charges and are therefore, from an electrochemical parameter viewpoint,[78,79] quite strong donors. Ligand **1** $(S \cdot SO_2)$ contains, formally, sulfur in oxidation states zero and +4 (sulfinyl), while in ligand **2** $(SO_2 \cdot SO_2)$ both sulfur atoms are S^{IV}.

Initially we used the popular B3LYP functional and LANL2DZ basis set but this led to an MO sequence that seemed inappropriate, yielded relatively poor bond distances compared with the X-ray data, and also led to electronic spectra that did not agree with the experimental data very well. Much better performance was achieved by using B3LYP with the triple-ζ basis TZVP for all atoms except ruthenium (absent from TZVP basis) where the double-ζ DGDZP basis set was used. Species **2** optimized to C_2

(73) Kholdeeva, O. A.; Kovaleva, L. A.; Maksimovskaya, R. I.; Maksimov, G. M. *J. Mol. Catal. A: Chem.* **2000**, *158*, 223–229.
(74) Lindsay Smith, J. R.; Gilbert, B. C.; Mairata i Payeras, A.; Murray, J.; Lowdon, T. R.; Oakes, J.; Pons i Prats, R.; Walton, P. H. *J. Mol. Catal. A: Chem.* **2006**, *251*, 114–122.
(75) Gamelas, C. A.; Lourenço, T.; Pontes da Costa, A.; Simplício, A. L.; Royo, B.; Romão, C. A. *Tetrahedron Lett.* **2008**, *49*, 4708–12.
(76) Feng, X.-M.; Wang, Z.; Bian, N.-S.; Wang, Z.-L. *Inorg. Chim. Acta* **2007**, *360*, 4103–110.
(77) De Rosa, M.; Lamberti, M.; Pellecchia, C.; Scettri, A.; Villano, R.; Soriente, A. *Tetrahedron Lett.* **2006**, *47*, 7233–35.
(78) Lever, A. B. P. *Inorg. Chem.* **1990**, *29*, 1271–1285.
(79) Lever, A. B. P.; Dodsworth, E. S. In *Inorganic Electronic Structire and Spectroscocpy*; J. Wiley and Sons: New York, 1999; Vol. 2, pp 227−287.

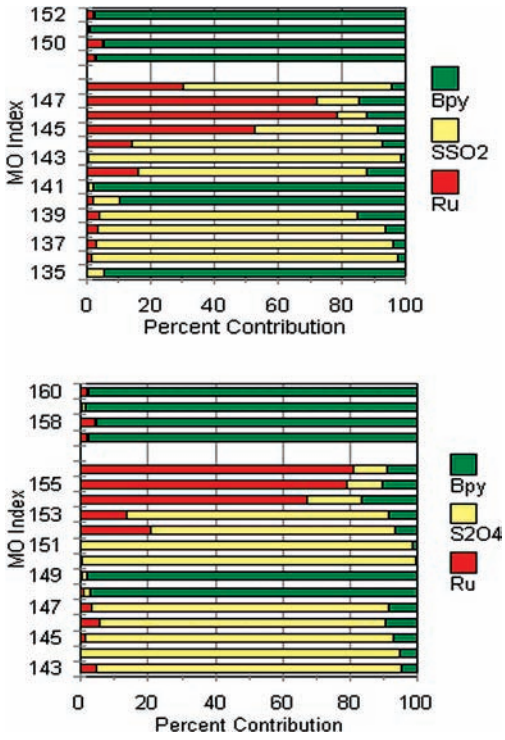

Figure 4. Relative contributions of Ru (red), S-ligand (yellow), and bipyridine (green) to the frontier orbitals of species **1** (upper) and species **2** (lower) (DFT, PCM acetonitrile- see text for details). The MO immediately below the white space is the HOMO and that immediately above, is the LUMO.

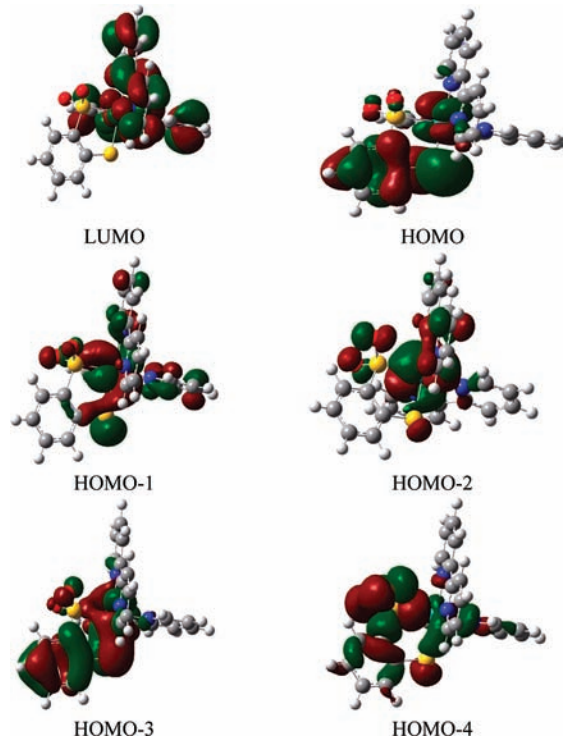

Figure 5. Frontier molecular orbitals of species **1**. [DFT B3LYP/TZVP and DGDZVP, PCM acetonitrile], see text for details. HOMO is orbital #148. The S-ligand lies to the lower left in these molecular orbitals and is easily identified through the yellow sulfur atoms.

symmetry. Key bond distances, summarized in Table 3, lay much closer to generally expected ranges and closer to the X-ray data for species **2**. This calculation yielded a frontier orbital sequence (Figure 4) where the highest filled orbitals are localized mainly on ruthenium and all importantly, as will be detailed below, when solvation was incorporated via the PCM,[61,62] the fit to the electronic spectrum became extraordinarily good.

The LUMO and the next five virtual orbitals (only three are shown) are predominantly antibonding orbitals of 2,2′-bipyridine. There are no low lying empty orbitals localized on the sulfur ligands; therefore we do not expect any lower energy MLCT bands to the S-ligands. In both species highest occupied molecular orbital (HOMO) to HOMO-2 have significant ruthenium 4d character, and are fairly pure (little mixing with S-ligand MOs) in species **2**. In the case of ($S{\cdot}SO_2$) species **1**, it is evident that the HOMO and HOMO-3 result from substantial coupling between Ru 4d and an S-ligand orbital. Indeed these two orbitals are bonding (HOMO-3) and antibonding (HOMO) combinations of the HOF_1O-1 of the [Ru(bpy)$_2$] fragment and the S-ligand HOF_2O-1.[80] Figure 5 displays the MOs of the complex and Figure 6 the MOs of the ($S{\cdot}SO_2$) ligand where it can be seen that HOF_2O-1 is localized on the S^0 atom with essentially no contribution from the S^{IV} atom. The complex HOMO-1 and HOMO-2 are seen to involve coupling of Ru(4d) to the S^{IV} atom, mostly to HOF_2O-2 and HOF_2O-4, respectively. Two other frontier orbitals contain appreciable Ru 4d contributions. HOMO-4 (#144) is formed by mostly

(80) The HOMO of fragment 1 is labeled as HOF_1O, the LUMO+1 of fragment 2, as LUF_2O+1, etc.

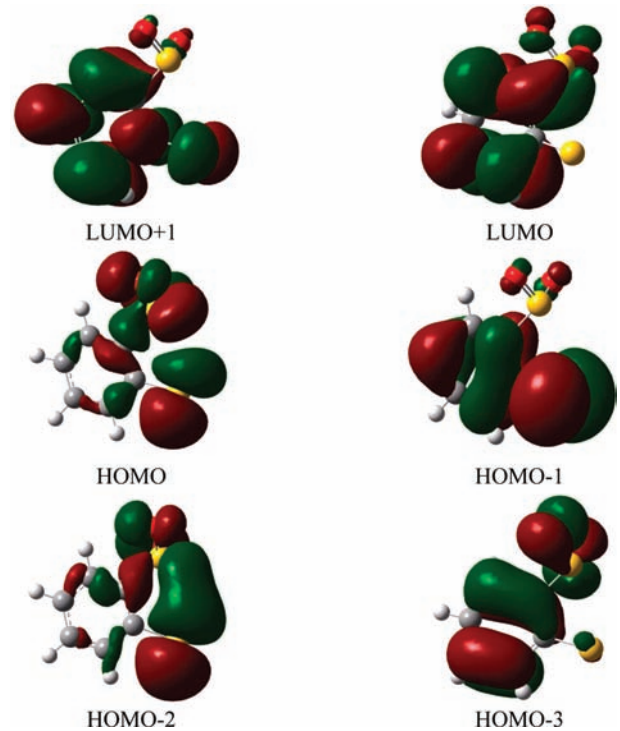

Figure 6. Frontier molecular orbitals of ($S{\cdot}SO_2$) ligand fragment. [DFT B3LYP/TZVP and DGDZVP, PCM acetonitrile], see text for details. HOMO is orbital #45.

a bonding interaction of S-ligand HOF_2O with the LUF_1O of the [Ru(bpy)$_2$] fragment, while HOMO-6 is mostly coupling of HOF_1O and HOF_2O-2.

In the case of species **2**, the first three frontier orbitals are associated with what would be the t_{2g} set in an octahedral

Table 4. Selected Bonding Data for Species **1,2**

	1 ($S^{\cdot}SO_2$)	**2**·($(SO_2)^{\cdot}(SO_2)$)
NBO charge on S-ligand, a.u.	−1.14	−1.13
NBO charge on Ru atom, a.u.	0.58	0.48
NBO charge on S atoms, a.u.	−0.28,1.67	1.67
NBO charge on Bipyridines, a.u.	0.56	0.65
NBO bond order Ru−S	0.86	n.a.
NBO bond order Ru−S(O_2)	0.84	0.85
ECDA charge on S-ligand (Mulliken), a.u.	−0.75	−0.72
Mulliken charge on Ru, a.u.	0.27	0.11
bond order [Ru(bpy)$_2$][S-ligand]	2.16	2.27
σ-donation from S-ligand, a.u.	1.36	1.44
back-donation to S-ligand, a.u.	0.14	0.18

field with HOMO, HOMO-1, and HOMO-2 mixed with the S-ligand HOF_1O-4, HOF_1O-5, and HOF_1O-1 in a bonding, antibonding, bonding interaction, respectively. MO data for the ($SO_2^{\cdot}SO_2$) complex and the ($SO_2^{\cdot}SO_2$) ligand and a detailed list of the percent contributions in the frontier orbitals of species **1,2**, can be found in Supporting Information, Tables S1, S2, and Figures S2, S3.

Using Extended Charge Decomposition analysis[60,81,82] the overall Mulliken charges on the S-ligand are the same for both ligands (Table 4) reduced from the formal −2 of the free ligand to about −0.75 au. This is seen to arise, after correction for polarization effects,[60] from a net σ-bond donation of approximately 1.4 au, and a very small back-donation of 0.1−0.2 au (Table 4). Using the alternate Natural Bond Orbital (NBO) method[83,84] similar trends are observed but with a somewhat more negative charge on the S-ligand and concomitantly, somewhat more positive charge remaining on Ru. Note especially, the very large difference in the NBO charges on S^0 (−0.28 au) and on S^{IV} (1.67 au).

Despite the clearly more covalent nature of the Ru−S^0 bond in **1** compared with Ru−S^{IV} in **1** and **2**, the overall bonding between Ru and these ligands is very similar. Figure 7 shows the bond orders for the other bonds in the complex, and one discriminatory feature does stand out. The bond orders of the Ru−N(bpy) bonds are all about 0.26−0.28 except for that *trans* to the $-S^0-$Ru bond, which is substantially larger (0.34), a clear *trans* effect. The C−S^0 bond order at 0.98 is substantially larger than that for C−S^{IV} (0.72 − 0.74) as would be expected given its much greater negative charge. To clarify issues relating to the electrochemistry, below, we also calculated (DFT) the properties of the first ($S = 1/2$) oxidation product of species **1.** This reveals considerable spin density on *both* the Ru and the S^0 atom (roughly equal, 0.44 spins) (not on $-S^{IV}$) to which it is attached. The $S = 1/2$ oxidation product of species **2** was also calculated using DFT, revealing that the Mulliken spin density is almost exclusively on the ruthenium atom with essentially zero spin density elsewhere.

Electrochemical Behavior

Complex **1** shows reversible oxidation at 0.42 V versus NHE, (Figure 8) and two distinct reversible waves in the negative region (−1.34 and −1.61 V). On the basis of the computational data these two negative region waves are clearly assigned as bpy/bpy^- of the first and second bpy ligand and lie in a typical potential range.[85,86] On the basis of the computational data above, the oxidation wave cannot be clearly assigned as either $Ru^{III/II}$ or ligand oxidation. However in the large group of complexes Ru(bpy)$_2$XY, there is a rough correlation between the $E_{1/2}$ [(bpy/bpy^-)] potential and the $E_{1/2}[Ru^{III/II}]$ potential,[86] and based thereon, 0.41 V is insufficiently positive to be assigned as a "simple" $Ru^{III/II}$ process. Given the extensive metal-S-ligand mixing in the HOMO of species **1**, and the spin density observed on both Ru and S in the oxidized species, one concludes that this redox process causes oxidation at both metal and ligand sites.[87] Thus, the ($S^{\cdot}SO_2$) ligand shows some non-innocent character.

Two processes associated with bipyridine reduction are also clearly observed in the voltammogram of species **2** at −1.28 and −1.54 V versus NHE, slightly less negative than the corresponding potentials for species **1**, and consistent with the slightly greater NBO positive charge on bipyridine in species **2** (Table 4). The oxidation process of **2** at 1.41 V versus NHE is shifted toward much more positive potential compared to **1** and lies in the expected region.[86] Given that the spin density of the oxidized product is now entirely localized on ruthenium, and the HOMO of species 2 is predominantly localized on ruthenium (Figure 4), the wave at 1.41 V is identified as the $E_{1/2}[Ru^{III/II}]$ process. Obviously the ($SO_2^{\cdot}SO_2$) ligand is more difficult to oxidize than the ($S^{\cdot}SO_2$) ligand. The ligand electrochemical parameter of the ($SO_2^{\cdot}SO_2$) ligand[78] can be derived from the observed $E_{1/2}$-$[Ru^{III/II}]$ potential of 1.41 V versus NHE, leading, with $E_L(bpy) = 0.259$ V, to $E_L(SO_2^{\cdot}SO_2) = 0.19$ V which is quite positive for a formally −2 charged ligand

Infrared Spectra

The experimental infrared spectra of these species are shown in Figure 9 and compared with the DFT calculated spectrum using B3LYP and the basis sets as described previously but excluding solvent. The agreement between theory and experiment is again remarkably good, without any need to scale the computed data. Selected calculated frequencies of species **1**, all strong except where noted, include: 409 cm^{-1} (vw) Ru−S stretch; 508 cm^{-1} SO_2 deformation; 574 cm^{-1} Ru−S(O_2) stretch; 983 cm^{-1} S−O symmetric stretch; 1105 cm^{-1} antisymmetric S−O stretch. These are the dominant vibrations but they are all fairly extensively coupled to other motion. The agreement between observed and predicted spectrum of species **2** is truly

(81) Frenking, G.; Frohlich, N. *Chem. Rev.* **2000**, *100*, 717–774.
(82) Gorelsky, I.; Solomon, E. I. *Theoret. Chim. Acc.* **2008**, *119*, 57–65; Erratum 67.
(83) Foster, J. P.; Weinhold, F. *J. Am. Chem. Soc.* **1980**, *102*, 7211–7218.
(84) Reed, A. E.; Curtiss, L. A.; Weinhold, F. *Chem. Rev.* **1988**, *88*, 899–926.
(85) Juris, A.; Balzani, V.; Barigelletti, F.; Campagna, S.; Belser, P.; Zelewsky, A. v. *Coord. Chem. Rev.* **1988**, *84*, 85–277.
(86) Haga, M.; Dodsworth, E. S.; Lever, A. B. P. *Inorg. Chem.* **1986**, *25*, 447–453.
(87) Grapperhaus, C. A.; Kozlowski, P. M.; Kumar, D.; Frye, H. N.; Venna, K. B.; Poturovic, S. *Angew. Chem., Int. Ed.* **2007**, *46*, 4085–88.

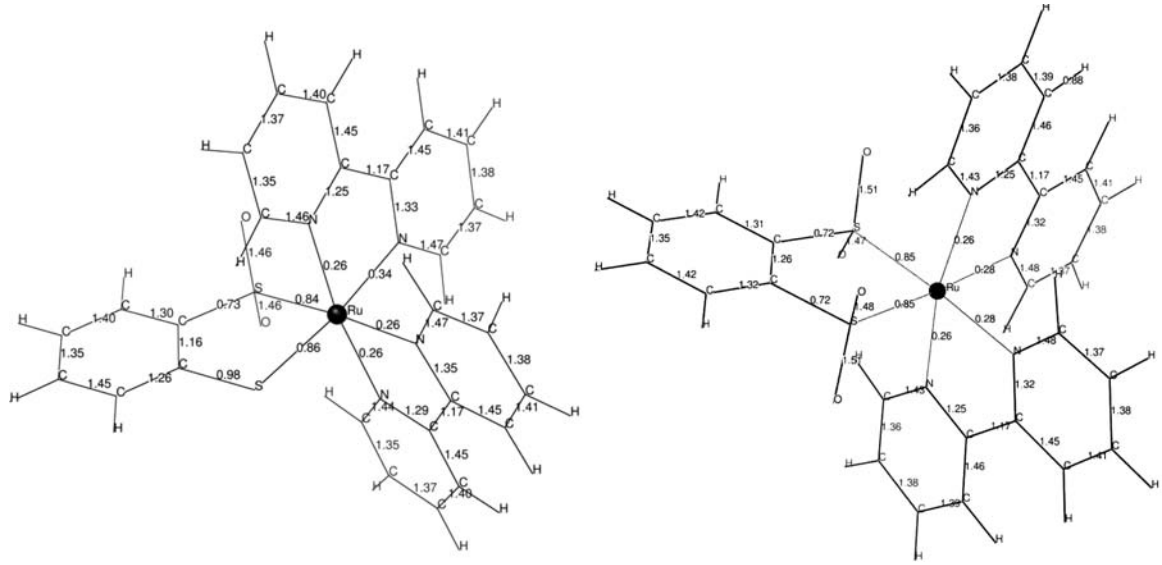

Figure 7. Mayer Bond Orders of (left) species **1** and (right) species **2** determined using DFT on the geometry optimized structures with the PCM as described in the text. Bond orders for the C−H bonds are all around 0.98 and are omitted.

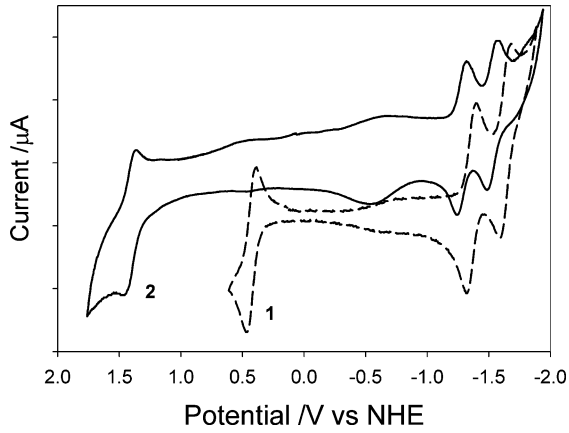

Figure 8. Cyclic voltammogram of $[Ru(bpy)_2(S\cdot SO_2\cdot)]$ (**1**) and $[Ru(bpy)_2(SO_2\cdot SO_2)]$ (**2**) in dimethyl formamide/$TBAPF_6$, scan rate 100 mV s^{-1}. The reference electrode was AgCl/Ag and was corrected to NHE using ferrocene (factor Fc^+/Fc at 0.69 V vs NHE).

excellent with an almost 1:1 correlation of observed and predicted bands. The intense band at 589 cm^{-1} is a mix of Ru−S symmetric stretch and an SO_2 deformation mode, while the weaker band at 561 cm^{-1} is the antisymmetric Ru−S mode coupled to an SO_2 deformation. The intense band at 989 cm^{-1} has both SO_2 units in a symmetric stretch but in an antisymmetric mode, that is, as one expands the other contracts, while that at 1119 cm^{-1} has the converse, that is, each SO_2 in an antisymmetric stretching vibration but coupled symmetrically. The assigned vibrations occur in the expected ranges.[88,89]

The isomeric disulfenate structure $Ru(bpy)_2(SO\cdot SO)$ as an alternative formulation of species **1** was excluded above, but to be sure, the infrared spectrum of this isomer was calculated. It is shown in Figure 9C. It is clearly very different from the spectrum of species **1** shown in Figure 9B. It displays a dominantly strong band at 871 cm^{-1} which

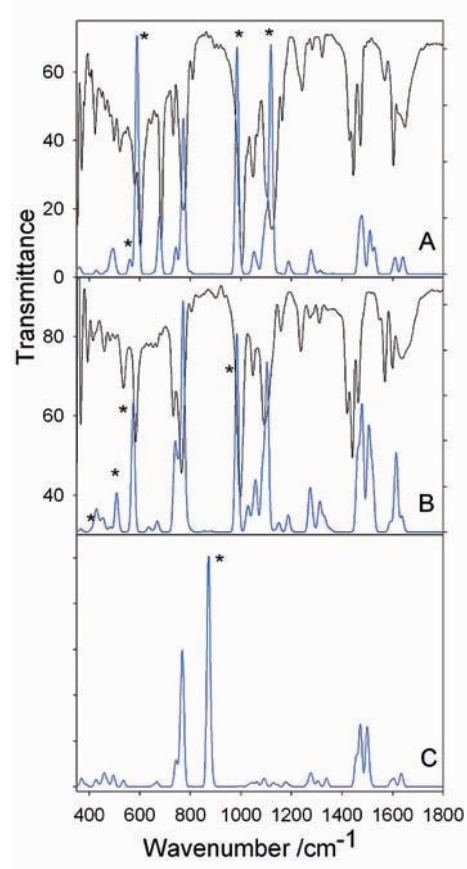

Figure 9. Experimental (black) and DFT computed (blue) infrared spectra of (A) species **2**, (B) species **1**, and (C) DFT computed spectrum (blue) of $Ru(bpy)_2(SO\cdot SO)$. Key bands noted in the text are identified with asterisks.

is the same type of asymmetric SO stretching vibration as that noted above for species **2** at 989 cm^{-1}. The corresponding symmetric S−O stretch is calculated as a very weak vibration at 883 cm^{-1}. Note that the experimental infrared spectrum of species **1** (Figure 9B) has no significant absorption near 870 cm^{-1}.

(88) Hesek, D.; Inoue, Y.; Everitt, S. R. L.; Ishida, H.; Kunieda, M.; Drew, M. G. B. *J. Chem. Soc., Dalton Trans.* **1999**, 3701–3709.
(89) Lauter, M.; Breitinger, D. K.; Breiter, R.; Mink, J.; Bencze, E. *J. Mol. Struct.* **2001**, *563−564*, 383–388.

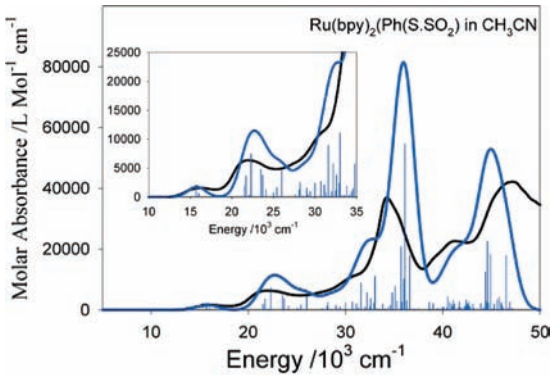

Figure 10. Optical spectrum of species **1** in acetonitrile. Experimental data are in black and the DFT derived data (PCM, acetonitrile) in blue. Peak half-width at half-height was 1200 cm^{-1} for all bands in the calculated spectrum. Vertical bars are the locations of the transitions with correct relative oscillator strengths normalized to the left-hand absorption axis. The inset shows expansion of the lower energy region for clarity.

Table 5. Principal Experimental Band Energies, Major Predicted Transitions and Assignments.

experimental 10^3 cm^{-1} (ε)	predicted major bands (f)	assignment
	$Ru(bpy)_2(S\cdot SO_2)$ **1**	
16.2(1550)	15.7(0.015)	#148→#149; Ru d,S → π^* bpy
22.0(6340)	22.3(0.06)	#146→#149, Ru d → π^* bpy
30.9sh	31.6(0.07)	v.mixed
34.2(37,000)	35.7(0.16)	#140→#150, π-π^* bpy
41.3sh		
47.2(42,150)	44.9(0.14)	#145→#159, Ru d, S → π^* bpy
	$Ru(bpy)_2(SO_2\cdot SO_2)$ **2**	
24.7(6510)	25.7(0.11)	#154→#157; Ru d → π^* bpy
35.2(40,000)	34.8(0.10);35.9(0.24)	v.mixed
40.0sh		
47.6(50,800)	44.5(0.12)	v.mixed

Optical Spectroscopy

Figure 10 compares the experimental visible region spectrum of species **1** (in CH_3CN) with the time dependent DFT[90,91] calculated spectrum of the DFT optimized geometry. The overall agreement is exceptionally good. The inclusion of solvent in the calculation is crucial; without this, the predicted visible region bands lie at appreciably higher energy. An example is shown in Supporting Information, Figure S1. Table 5 lists the principal experimental band energies and the strongest predicted transitions. A complete set of predicted transitions can be found in Supporting Information, Table S3. There are clearly a large number of overlapping transitions and, up to about 25,000 cm^{-1}, they are described either as S-ligand→ π^* bpy LLCT or Ru d → π^* bpy MLCT or a mix thereof. The lower energy band at 16,200 cm^{-1} is a mix of both these transitions, while the stronger band at 22,000 cm^{-1} is mostly the expected Ru 4d → π^* bpy MLCT. The strong peak at 34,200 cm^{-1} is predominantly π-π^* bpy but it is evident that the observed spectrum is a composite of very many transitions (Table 5 and, Supporting Information, Table S3).

Figure 11 compares the experimental visible region spectrum of species **2** (in CH_3CN) with the DFT calculated spectrum of the DFT optimized geometry. The overall agreement is again exceptionally good. The lower energy weak band seen in the spectrum of species **1**, is, of course, now absent since **2** does not contain an S^0 atom. The band at about 25,000 cm^{-1} is the expected Ru 4d → π^* bpy MLCT. Once again there are many overlapping transitions; in this case it is not even possible to define the nature of the stronger bands since they are a composite of many electronic excitations (Table 5, and in Supporting Information, Table S4).

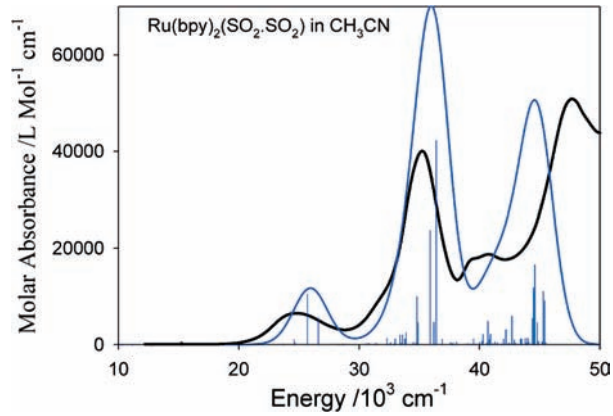

Figure 11. Optical spectrum of species **2** in acetonitrile. Experimental data are in black and the DFT derived data (PCM, acetonitrile) in blue. Peak half-width at half-height was 1500 cm^{-1} for all bands in the calculated spectrum. Vertical bars are the locations of the transitions with correct relative oscillator strengths normalized to the left-hand absorption axis. The calculated spectrum terminates at about 46,000 cm^{-1}. Better agreement with the higher energy uv region could probably have been derived from a much more time intensive CPU calculation of transitions beyond 46,000 cm^{-1} but the reliability of such a high energy calculation is suspect.

Summary

We have reported in some considerable detail the geometric and electronic structures of ruthenium complexes of two sulfinate ligands which have only comparatively rarely been studied. The presence of an S^0 ligator in one complex confers some non-innocent character on this ligand, a feature which will be explored in further detail elsewhere.[92] Despite the difference in net oxidation states of the two ligands, the electronic structures of the ruthenium species are fairly similar. However the Ru−S^0 bond is significantly more covalent than the Ru−S^{IV} bond and exerts a *trans* effect on the Ru−N bond across from it. The optical spectra of these species are apparently similar except for the observation of a low energy, weak S^0 → π^* bpy transition observed in species **1** but obviously not in **2**. The apparent simplicity of the UV/vis optical spectra insofar as only a small number of transitions are apparently seen, belies the complexity of these systems whereby there are an impressive number of actual electronic transitions lying underneath the simple band envelope. Many of these transitions also derive from excitations between several pairs of molecular orbitals. These data should prove useful in the elucidation of the structure and function of the *nitrile hydratase* metalloenzymes.

(90) Vlcek, A., Jr.; Záliš, S. *Coord. Chem. Rev.* **2007**, *251*, 258–287.
(91) Daniel, C. *Coord. Chem. Rev.* **2003**, *238*−*239*, 143–166.
(92) Lever, A. B. P. *Can. J. Chem* 2009, submitted for publication.

Acknowledgment. The authors thank the Natural Sciences and Engineering Research Council (Ottawa) for financial support, and the Johnson-Matthey company for the loan of ruthenium trichloride. This work was made possible by the facilities of the Shared Hierarchical Academic Research Computing Network (SHARCNET: www.sharcnet.ca).

Supporting Information Available: More detailed molecular orbital and optical spectroscopic data, and the complete author listing of ref 44. This material is available free of charge via the Internet at http://pubs.acs.org. The crystal structure of species **2** has been deposited in the Cambridge Structural Database as CCDC 704806.

IC801898T